JPhys Materials

PAPER • OPEN ACCESS

How to grow single-crystalline and epitaxial NiTi films in (100)- and (111)-orientation

To cite this article: Klara Lünser *et al* 2023 *J. Phys. Mater.* **6** 035002

View the article online for updates and enhancements.

You may also like

- A novel active fire protection approach for structural steel members using NiTi shape memory alloy
H Sadiq, M B Wong, R Al-Mahaidi et al.
- Experimental evaluation of SMA-based multi-ring damping devices
Mohammad Salehi, Darel Hodgson, T Kim Parnell et al.
- Fatigue tests of superelastic NiTi wires: an analysis using factorial design in single cantilever bending
Magna Silmara de Oliveira Araújo, Estephanie Nobre Dantas Grassi and Carlos José de Araújo

This content was downloaded from IP address 194.95.157.48 on 12/10/2023 at 13:53

Journal of Physics: Materials

PAPER

How to grow single-crystalline and epitaxial NiTi films in (100)- and (111)-orientation

Klara Lünser[1,2,3,*], Andreas Undisz[4,5], Kornelius Nielsch[2,3] and Sebastian Fähler[1]

[1] Helmholtz-Zentrum Dresden-Rossendorf, Institute of Ion Beam Physics and Materials Research, Bautzner Landstr. 400, 01328 Dresden, Germany
[2] Leibniz IFW Dresden, Institute of Metallic Materials, Helmholtzstr. 20, 01069 Dresden, Germany
[3] TU Dresden, Institute for Materials Science, Helmholtzstr. 7, 01069 Dresden, Germany
[4] TU Chemnitz, Institute of Materials Science and Engineering, Erfenschlager Str. 73, 09125 Chemnitz, Germany
[5] Friedrich-Schiller Universität Jena, Otto Schott Institute of Materials Research, Loebdergraben 32, 07743 Jena, Germany
[*] Author to whom any correspondence should be addressed.

E-mail: k.luenser@hzdr.de

Keywords: NiTi films, shape memory alloys, epitaxial film growth, nitinol

Supplementary material for this article is available online

OPEN ACCESS

RECEIVED
1 December 2022

REVISED
9 May 2023

ACCEPTED FOR PUBLICATION
16 May 2023

PUBLISHED
26 May 2023

Original Content from this work may be used under the terms of the Creative Commons Attribution 4.0 licence.

Any further distribution of this work must maintain attribution to the author(s) and the title of the work, journal citation and DOI.

Abstract

Understanding the martensitic microstructure in nickel–titanium (NiTi) thin films helps to optimize their properties for applications in microsystems. Epitaxial and single-crystalline films can serve as model systems to understand the microstructure, as well as to exploit the anisotropic mechanical properties of NiTi. Here, we analyze the growth of NiTi on single-crystalline MgO(100) and Al_2O_3(0001) substrates and optimize film and buffer deposition conditions to achieve epitaxial films in (100)- and (111)-orientation. On MgO(100), we compare the transformation behavior and crystal quality of (100)-oriented NiTi films on different buffer layers. We demonstrate that a vanadium buffer layer helps to decrease the low-angle grain boundary density in the NiTi film, which inhibits undesired growth twins and leads to higher transformation temperatures. On Al_2O_3(0001), we analyze the orientation of a chromium buffer layer and find that it grows (111)-oriented only in a narrow temperature range around 500 °C. By depositing the Cr buffer below the NiTi film, we can prepare (111)-oriented, epitaxial films with transformation temperatures above room temperature. Transmission electron microscopy confirms a martensitic microstructure with Guinier Preston-zone precipitates at room temperature. We identify the deposition conditions to approach the ideal single crystalline state, which is beneficial for the analysis of the martensitic microstructure and anisotropic mechanical properties in different film orientations.

1. Introduction

Nickel–titanium (NiTi) films are an important material for micro-actuators [1–4] and for elastocaloric refrigeration [5]. Their functionalities originate from a martensitic transition between cubic B2 austenite and monoclinic B19′ martensite. Films are mostly produced as polycrystals by depositing NiTi onto substrates such as SiO_2 or Si at room temperature and crystallizing the initially amorphous films by annealing [6–11]. The film's transformation behavior depends on the film composition as well as the heat treatment time and temperature, because different precipitates like $NiTi_2$, Ni_4Ti_3 or Guinier Preston (GP) zones can occur [8, 12–14]. Depending on the deposition conditions, the film can have a one-step transformation directly from B2 to B19′ or a two-step transformation, where the additional R-phase occurs as an intermediate step.

Although polycrystalline films are well suited for most applications, some mechanical properties such as the stress–strain behavior [15], crack growth [16], hardness and indentation modulus [17] and even the elastocaloric response [18] are anisotropic and could therefore benefit from single-crystalline films.

© 2023 The Author(s). Published by IOP Publishing Ltd

Moreover, studying the martensitic microstructure is facilitated when no large-angle grain boundaries are present, as the grain boundaries influence the martensitic transformation. One possibility of achieving films without large-angle grain boundaries is by growing epitaxial films. An epitaxial film is a film that grows with a well-defined orientation relation between the film and the substrate crystal lattice. As such, epitaxial films represent the film counterpart of single crystals and are therefore beneficial to study both, the anisotropy of mechanical properties and the martensitic microstructure. This approach has been applied to other martensitic materials like Ni–Mn–Ga already, where epitaxial films have helped to understand the electronic origin of the martensitic transformation [19], the nucleation of martensite [20] and the hierarchical martensitic microstructure [21]. As these films are prepared at elevated temperatures in the austenite phase, the term 'epitaxial' refers to this state. During cooling, the austenite transforms to several variants of the martensite, creating twin boundaries. It is therefore worth to point out that the transformed, martensitic films, although epitaxially grown, are not anymore single-crystalline in a strict sense. So far, epitaxial NiTi films have been produced on GaAs(100) with molecular beam epitaxy (MBE) [22], and on MgO(100) with MBE [23] and with sputter deposition [24, 25]. In all cases, the films grow (100)-oriented with an orientation relationship of MgO/GaAs(100) [001] ||NiTi B2(100) [011]. However, the films produced with sputter deposition were austenitic at room temperature and the films produced by MBE were only 35 nm thin. Therefore, none of these films can be used to analyze the microstructure and the shape memory properties at room temperature. Moreover, films in a different orientation then (100) could offer more possibilities to measure anisotropic properties in more directions.

Here, we provide deposition routes to grow epitaxial NiTi films in two different orientations: (100) and (111). We use the results from [24] as a starting point to optimize the film growth on MgO(100) by using an additional buffer layer between film and substrate and analyze the effect of the buffer layer on crystal quality and transformation behavior. In addition, we present a way to grow (111)-oriented films by using Al_2O_3(0001) substrates and an optimized buffer layer. We show that the films in both orientations grow in a single orientation and contain only a low density of small-angle grain boundaries, meaning that they approach the ideal single crystal state. Moreover, the films exhibit transition temperatures above room temperature.

2. Materials and methods

For film preparation, we used DC Magnetron sputter deposition with a $4''$ $Ni_{46.8}Ti_{53.2}$-target. The base pressure before sputtering was $<10^{-9}$ mbar and during sputtering, a mix of Ar and 5 vol% hydrogen with a pressure of 8×10^{-3} mbar was used. The buffer layers were sputtered from $2''$ Cr and V elemental targets by Kurt J. Lesker. NiTi was sputtered with a power of 100 W, Cr with 70 W and V with 150 W. A 5 nm Cr buffer layer was deposited below all buffer layers for adhesion. During deposition, the substrate holder was rotated to ensure homogeneous thickness. The substrate was heated during depositions; the deposition temperatures for particular samples are given in the text. Some samples were annealed directly after deposition in the sputter chamber. As substrates, we used 1×1 cm single-crystalline MgO(100) and Al_2O_3(0001) substrates from Crystec GmbH. The film composition can be adapted by changing the distance between the target and the substrate [6]. By decreasing this distance, the Ti-ratio increases. For scanning electron microscopy and to determine the chemical composition with energy dispersive x-ray spectroscopy, a LEO 1530 Gemini microscope by Zeiss was used. The composition was measured with an XFlash Detector from Bruker with an accuracy below 1 at%. Pole figures and rocking curves were measured with a Philips X'Pert using Cu–K_α-radiation. For pole figures, the parameters ranged from $0° \leqslant \phi \leqslant 360°$ and $0° \leqslant \chi \leqslant 90°$ with a step size of 1°. The rocking curves were measured at the B2(200) reflection with $\Delta\omega$ ranging from $-3°$ to 3° and a step size of 0.01°. We used x-ray diffraction (XRD) in Bragg–Brentano geometry with a Bruker D8 x-ray diffractometer using Co–K_α radiation of $\lambda = 0.178\,997$ nm. 2θ ranging from 20° to 100° was measured with a stepsize of 0.02° and 1 s $step^{-1}$. To index XRD measurements, we used the following lattice parameters: [26] B2 $a_0 = 0.3015$ nm, B19' $a = 0.2885$ nm, $b = 0.4120$ nm, $c = 0.4622$ nm and $\beta = 96.8°$. The surface topography was characterized with atomic force microscopy (AFM) in tapping mode using an ICON AFM by Bruker. Measurement data was analyzed with the software WSxM [27] and the rough mean square root (RMS) was determined from a 20×20 µm image. To analyze the transformation behavior, a physical property measurement system (PPMS) was used. The resistivity as a function of temperature was measured in four-contact geometry with a current of 1 mA and a cooling/heating speed of 3 K min^{-1}. The transformation temperatures for all films, which were determined from the resistivity measurements, can be found in the supplementary in table S1. For transmission electron microscopy (TEM) measurements, a

lamella was cut out of the film using focused ion beam with a FEI Helios NanoLab 600i. TEM was carried out using a NEOARM 200 F by JEOL with a voltage of 200 kV in scanning-TEM mode.

3. (100)-oriented NiTi films on MgO(100)

For epitaxial films, the misfit between the film and the substrate can have a tremendous influence on the growth behavior, the resulting microstructure and the film's properties [28]. This is because the misfit can cause lattice strain and/or the formation of dislocations. By depositing a buffer layer with desired lattice parameters between the substrate and the film, the misfit can be tuned. To analyze the effect of the misfit on the microstructure and transformation behavior of (100)-oriented epitaxial NiTi films, we deposited 400 nm NiTi on bare MgO substrates as used by [24] as well as on Cr- and V buffer layers. We chose V as the candidate having very similar lattice parameters to the B2 NiTi austenite, resulting in a misfit of only 0.4%. We also used Cr, which increases the misfit to −4.7%. Since V and Cr are miscible, the lattice parameter can be tuned between that of Cr and that of V by mixing both in a specific ratio. With a V to Cr ratio of 83 at% to 17 at%, we achieved a misfit of −1.3%. To compare the influence of the metallic buffer layer to the oxidic substrate, we also analyzed a film deposited on bare MgO(100), equally creating a misfit of −1.3%. All buffer layers were grown at 300 °C. 400 nm NiTi were then grown at 250 °C, followed by a two-step annealing according to [24] (2 h at 650 °C, 20 min at 300 °C). The film composition of $Ni_{52}Ti_{48}$ was chosen to give austenitic films at room temperature, to ensure an easy analysis of orientation and roughness. In XRD measurements, all films only show (*l*00) peaks from the substrate, buffer and B2 NiTi, without any peaks from precipitates or other phases (see supplementary, figure S1). This proves that the films grow with a (100)-texture on MgO(100).

Figure 1 summarizes the influence of different buffer layers on the crystal quality, the transformation behavior and the morphology of the NiTi films. Rocking curves (figure 1(a)) give insight into the crystal quality and the dislocation density of a film, because the curves become broader when more crystallites in the film are slightly misaligned. The full width at half maximum (FWHM) was extracted from each curve and the data is plotted in figure 1(b). Looking only at the films with metallic buffer layers, the crystal quality indeed decreases with an increased (absolute) misfit: The FWHM for the film with Cr buffer is 0.47°, for the film with V–Cr buffer it is 0.16° and for the film with V buffer 0.13°. However, this observation is only true when comparing different metallic buffers. The bare MgO substrate, although having a low misfit of −1.3% with respect to the film, produces a film with a much lower crystal quality than the Cr buffer with a large misfit of −4.7%. This means that two different influences have to be considered: the misfit, and whether the film grows on a metallic buffer or on an oxidic substrate. We suggest that this drastic change in crystal quality with buffer layer compared to without comes from the different conditions in the initial state of the deposition. Although the substrate heater is set to 250 °C for the film deposition in all cases, in contrast to a metallic buffer, a bare oxide MgO substrate is transparent to radiated heat and will therefore be much colder. At lower temperatures, less diffusion can take place, thus, more defects remain, which leads to a larger misorientation of the crystals in the beginning of the deposition. When these first crystals grow together, their orientation difference leads to small-angle grain boundaries and therefore a larger dislocation density.

The buffer layer and misfit also have an influence on the roughness of the NiTi films. AFM micrographs are shown in the supplementary (figure S2), the roughness extracted from them is summarized in figure 1(b). Whereas the roughness of the films on V and V–Cr are similar, the roughness of the film on Cr is much higher. Similar to the crystal quality, the roughness of the film on MgO can be decreased by depositing V–Cr below. This indicates that the film roughness can be attributed to the small-angle grain boundaries.

In figure 1(c), the influence of the crystal quality on the transformation behavior is shown. The film grown directly on MgO has a two-step transformation behavior during cooling and heating. In the resistivity measurement, the two-step transformation is visible as sharp rise and subsequent decrease in the resistivity which comes from the transformation to and away from the R-phase [29]. In contrast, the films on V (and V–Cr) exhibit a one-step transformation, and the transformation temperatures are higher. Following [30], these tendencies can be explained with the lower dislocation density because especially the R → B19′ transformation is hindered by dislocations. This is because high densities of dislocations hinder lattice distortions, which are an integral part of the martensitic transformation. The effect is much stronger for the B19′ transformation because the lattice distortion is larger compared to R-phase [31]. Therefore, the martensitic start temperature is shifted to lower temperatures while the R-phase start temperature remains fairly constant. With a buffer layer, the dislocation density is decreased, causing the transformation temperatures to be higher. The transformation curve of the film on Cr (blue curve) shows a different transformation behavior, with a gradual rise of the resistivity upon cooling from 276 K to 157 K. As this

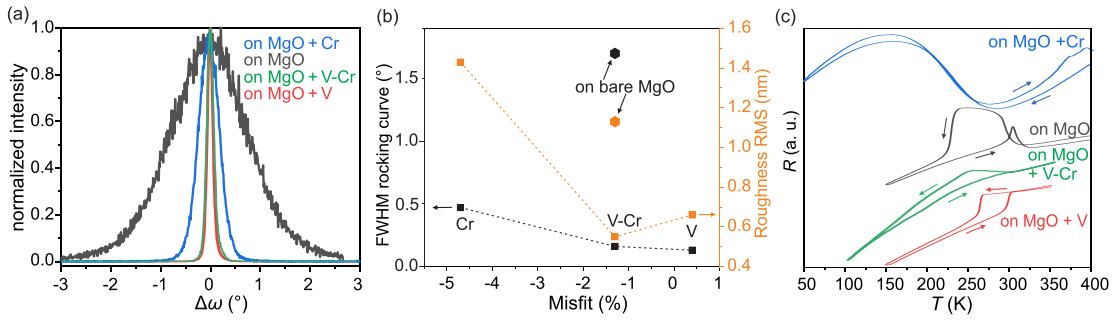

Figure 1. Influence of a buffer layer on crystal quality, transformation behavior and roughness of (100)-oriented $Ni_{52}Ti_{48}$ films on MgO(100). All buffers have a 5 nm Cr buffer below for adhesion to the substrate. (a) The rocking curves around the B2(200) reflex show that the misorientation is highest for the sample without a buffer (black curve), smaller for the sample on Cr (blue curve) and even smaller for samples on V–Cr and V (green and red curve). This shows that the misorientation and therefore the crystal quality are not so much determined by the misfit, but depend much more on whether the film is deposited onto a metallic buffer or onto an oxide substrate. (b) Full width at half maximum (FWHM, black dots) extracted from rocking curves and roughness (RMS, orange dots) extracted from AFM micrographs (see supplementary figure S1). To illustrate the trends for the films with buffer layer, we connected the data points for these samples with dashed lines. Both the crystal quality and the roughness depend on the misfit, but are higher for the sample without buffer. (c) Temperature dependent resistivity curves summarize the influence of the crystal quality on the transformation curves. With higher crystal quality, the transformation temperatures are shifted to higher temperatures and the transformation goes from a two-step transformation to a one-step transformation. Arrows mark the measurement directions.

transformation has a small hysteresis, it is likely that the film only transforms from B2 to R-phase and not to B19′. Our analysis reveals that a V buffer is most suitable for single-crystalline (100) films because of the low misfit to NiTi and because compared to bare oxidic substrates, a metallic buffer layer leads to higher temperatures during film growth and to a better crystal quality.

For applications of NiTi films, film thicknesses higher than 400 nm are of interest. Therefore, we analyzed the growth of a 1600 nm thick NiTi film on MgO(100). Compared to the films in figure 1, these films were grown with a smaller target to substrate distance during deposition, which results in Ti-rich films ($Ni_{48}Ti_{52}$). In figure 2, we analyze the epitaxial growth relation of two films in more detail. Figure 2(a) shows the XRD measurement of a film on MgO without buffer layer. We show XRD measurements in Bragg–Brentano geometry, which are a common and intuitive measurement of a film's texture. These measurements can reveal the present phases and their alignment perpendicular to the substrate, but do not give their orientation within the film plane, required to prove the epitaxial growth of a film. In this case, the sole appearance of one MgO(200) and one B2(200) peak shows a strong (100)-texture of the film. To prove the epitaxial growth of a film, we measured pole figures, which show the orientations of a specific lattice plane and can unambiguously clarify the epitaxial relation of the film to the substrate. On MgO without a buffer layer, the expected (100) epitaxial orientation is visible. Additionally, the films show intensity maxima in the pole figure that do not correspond to the desired (100) epitaxial orientation but stem from growth twins instead (figure 2(a)). These $\{112\}_{bcc}\langle 11\bar{1}\rangle_{bcc}$ growth twins have been observed in epitaxial NiTi films before [24]; they are a common deformation twinning mode in bcc metals [32]. We propose that the larger misorientation between grains or the higher dislocation density in the films grown without a buffer layer lead to the nucleation of these growth twins. Moreover, the thick film without buffer shows a broad transformation that includes the R-phase during cooling (figure 2(a), right). However, by growing films with the additional V buffer layer, the growth twins no longer appear (figure 2(b)), indicating that the crystal quality is a decisive factor. We observe a splitting of the epitaxial reflections, which we attribute to a slight shear occurring during the martensitic transformation. Indeed, as evident from the $R(T)$ measurement in figure 2(b), the buffer layer leads to higher transformation temperatures, smaller transformation temperature intervals (i.e. the difference between M_S and M_F or between A_S and A_F, respectively) and reduces the occurrence of the R-phase. Also the XRD measurement in figure 2(b) shows that a martensitic transformation has taken place. The B2(200) peak has partly split up into B19′(022) and B19′(200). The appearance of (022) is due to the lattice correspondence of B2 and B19′, where B2[002] corresponds to B19′[220] [33]. Including a V buffer layer underneath NiTi films on MgO consequently helps to increase both, the epitaxial growth and the transformation temperatures.

With our research on (111)-oriented films, we realized that NiTi also grows epitaxially and (100)-oriented when deposited at 525 °C on Cr (grown at 500 °C) on MgO(100). These deposition conditions will be further described in the next chapter. As these films do not require any annealing, we used them as an opportunity to analyze the influence of the annealing on the film properties. Figure 3 shows the

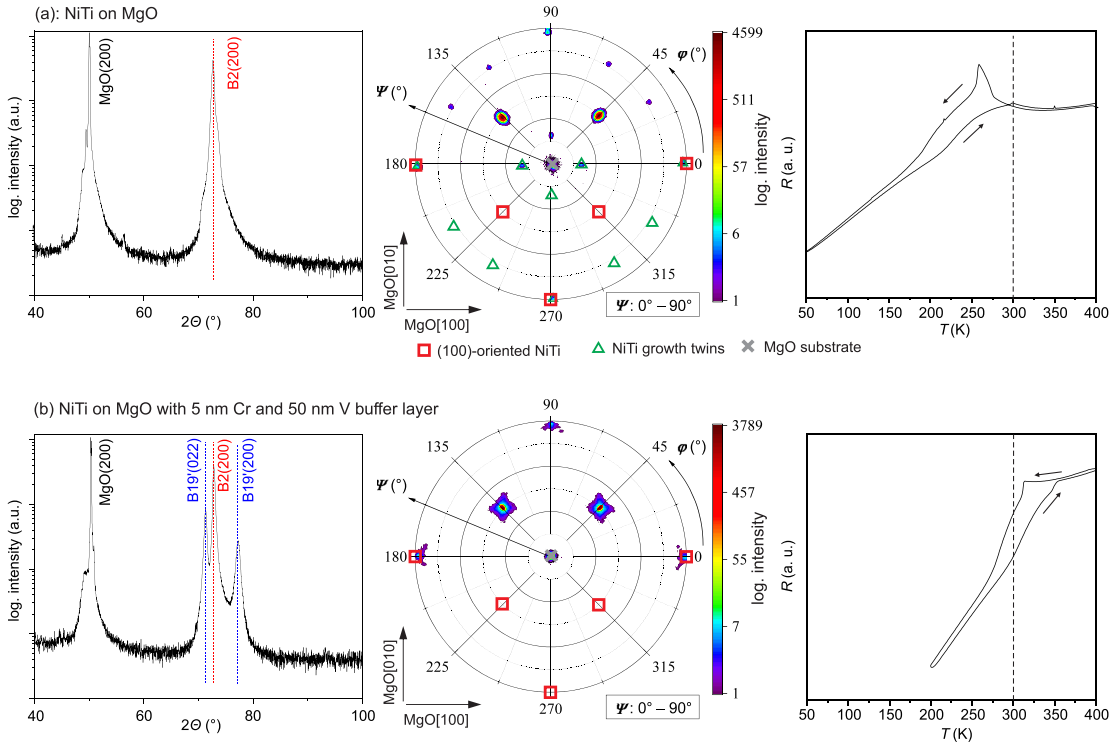

Figure 2. Orientation and transformation behavior of 1600 nm thick $Ni_{48}Ti_{52}$ films growth (a) directly on MgO and (b) with 5 nm Cr and 50 nm V buffer layer. (a) The XRD in Bragg–Brentano geometry shows only the MgO(200) and NiTi B2(200) peak and therefore a strong (100)-texture of the film. The measured B2(110) pole figure (upper half) shows that most of the film grows (100)-oriented (marked as red squares in the calculated pole figure in the lower half), but additional maxima from $\{112\}_{bcc}$ growth twins (green triangles) are visible as well. The pole figures were taken at room temperature. The transformation curve (right) of this film reveals a two-step transformation B2 → R → B19′ during cooling and a one-step transformation during heating. In both cases, the transformation spans over 100 K. (b) With additional Cr- and V buffer layer, the XRD shows B19′ peaks in addition to the MgO(200) and B2(200) peak, hinting that the film is partially martensitic. The B2(200) peak splits up into B19′(200) and B19′(022) due to the lattice correspondence between B2 and B19′. In the pole figure, the growth twins disappear. Compared to (a), the transformation temperatures are shifted to higher temperatures, the transformation is one-step also during cooling and transformation temperatures intervals are smaller. The dotted lines mark room temperature.

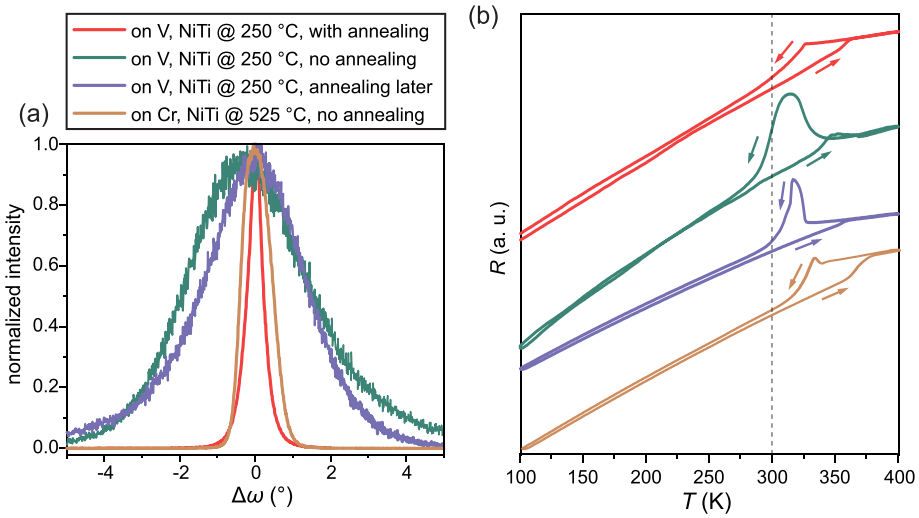

Figure 3. Influence of different deposition and annealing conditions on crystal quality and transformation behavior of 3000 nm thick, epitaxial NiTi films on MgO(100). (a) Rocking curves of the films show that either a direct annealing or a deposition at high temperatures is necessary to achieve a high crystal quality. Without annealing or with annealing after film oxidation, the crystal quality is low. (b) The crystal quality influences the temperature dependent resistivity curves of films. With good crystal quality, the transformation is within a narrower temperature interval and at higher temperatures. Arrows denote the measurement direction.

influence of different deposition and annealing conditions on crystal quality and transformation behavior. We compare four different films, all with 3000 nm thickness: The first film was deposited with the deposition conditions mentioned in the last paragraphs. NiTi was grown at 250 °C on V with a two-step post-annealing directly in the sputter chamber (red curves in figure 3). The second sample was prepared with the same deposition conditions, but without any post-annealing (green curve). The third film was identical to the second film, however, it was post-annealed a day later, after having been in ambient air for a night (purple curve). The fourth film was deposited on a Cr buffer grown at 500 °C and the film's deposition temperature was 525 °C without any annealing (brown curve). Both rocking curve and transformation behavior substantially differ depending on the deposition conditions. The rocking curve in figure 3(a) is significantly wider for the film without heat treatment (green curve) than with heat treatment (red curve). This suggests that the crystal quality is improved with the heat treatment, because the high annealing temperatures of 650 °C and the time of 2 h provide enough energy and time for sufficient diffusion. Similar to the previous comparisons of different buffer conditions, the crystal quality influences the transformation behavior (figure 3(b)): with annealing, the film shows a one-step transformation, without annealing a two-step transformation via the R-phase during both cooling and heating. It is interesting to note that the deposition temperature of 250 °C is below the crystallization temperature of NiTi (about 450 °C [8, 34]), still, the film does not grow amorphously. When the heat treatment is performed after breaking the vacuum, the Rocking curve and thus the misorientation hardly differs from that without heat treatment (purple curves in figure 3). Accordingly, a direct heat treatment increases the crystalline quality of the film, but a subsequent heat treatment does not. We propose that this is a result of the surface oxidation with the ambient air. Presumably, the oxidation layer prevents unhindered crystallization during subsequent heat treatment, which means that the condition after deposition largely remains. Accordingly, the transformation is slightly sharper than without annealing, but the R-phase still occurs during cooling. For comparison, the brown curves in figure 3 show the film which was directly deposited at high temperatures of 525 °C without any annealing. The rocking curve is very similar to the annealed film. Also, the transformation is, apart from a very small peak in the cooling curve indicating the R phase, comparable. This means that a post-annealing is not necessary if the films are deposited at sufficiently high temperatures.

For growing (100)-oriented, epitaxial NiTi films, two deposition routes work—either depositing NiTi at 250 °C on a V buffer, followed by a two-step annealing or depositing NiTi at 525 °C on a Cr buffer without annealing. If it is not necessary to have a clear one-step transformation, the deposition at higher temperatures turned out to be more user-friendly, as it is quicker, simpler and more reliable. It is worth to note that the influence of misfit on crystal quality and transformation behavior is smaller when films are deposited at 525 °C compared to 250 °C. At higher deposition temperatures, the increased diffusivity facilitates accommodating the misfit by introducing misfit dislocations during growth. This explains why growing epitaxial films using a Cr buffer works better when depositing Cr and NiTi at 500 °C and 525 °C compared to the 300 °C and 250 °C as described before.

4. (111)-oriented NiTi films on Al_2O_3(0001)

To have an additional fundamental orientation available for experiments, we now aim to grow (111)-oriented films. This allows to probe mechanical properties in additional directions and makes it possible to compare the martensitic microstructure of films to (111)-textured bulk NiTi [35, 36]. Al_2O_3(0001) is a possible substrate for (111)-oriented films, as it provides a three-fold symmetry. However, growing films on Al_2O_3(0001) with the same deposition conditions as for MgO(100) resulted in polycrystalline films which are mostly (110)-oriented (see supplementary figure S3). Therefore, we went back one step and first investigated the growth of a Cr buffer layer on Al_2O_3(0001). The idea behind this is that NiTi should reproduce the orientation of the Cr-buffer, therefore we need to identify deposition conditions under which the Cr grows (111)-oriented.

Figure 4 shows how the orientation and morphology of a 50 nm thick Cr buffer on Al_2O_3(0001) change with the deposition temperature T_{Dep}. At T_{Dep} of 300 °C (figure 4(a)), the buffer grows textured in several (110)-orientations (purple circles), whereas the desired (111)-orientation (red squares) is barely present. Under these deposition conditions, the buffer grows with tiny lateral features of only some nm, and with a roughness (RMS) of 1.93 nm the buffer is quite smooth. When the deposition temperature is increased to 450 °C (figure 4(b)), the (111)-orientation (red squares) begins to appear more pronounced, while the RMS (3.28 nm) and the feature size increase. At T_{Dep} of 500 °C (figure 4(c)), the (111)-orientation dominates and the other orientations are only visible due to the logarithmic intensity scale. At this T_{Dep}, a further increase in roughness (RMS = 7.8 nm) is observed. By increasing the deposition temperature to 600 °C (figure 4(d)), the (111)-orientation completely disappears again, leaving a fully (110)-oriented buffer. Although this buffer

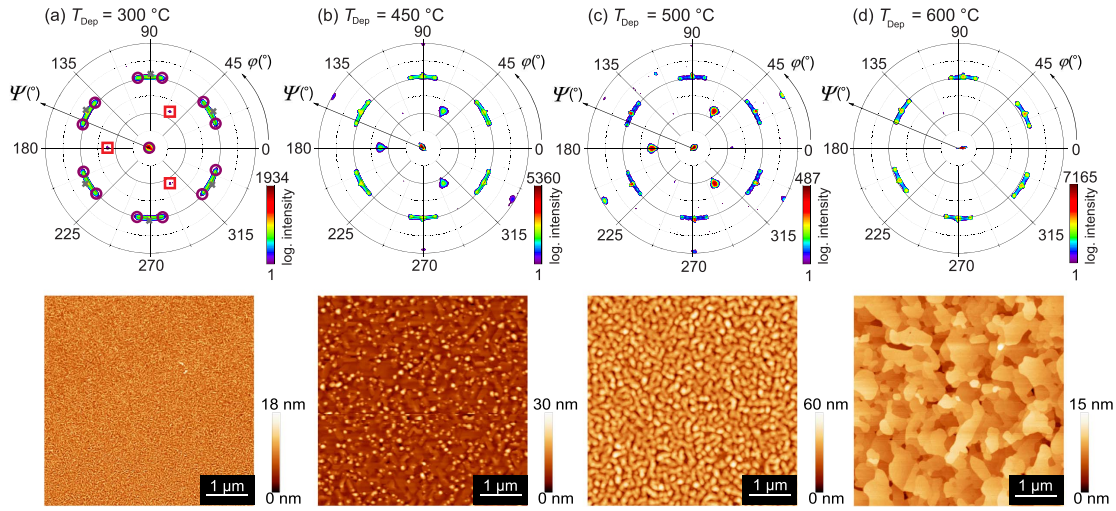

Figure 4. Orientation and morphology of Cr-Buffer layer on $Al_2O_3(0001)$ for different deposition temperatures T_{Dep}. The Cr(220) pole figures (first row) show that the orientation of the Cr buffer depends on the deposition temperature. For 300 °C and 600 °C, the buffer grows (110)-oriented (purple circles), for 450 °C in a mix of (110) and (111)-oriented, whereas at 500 °C it grows mostly in the intended (111)-orientation (red squares). Gray crosses mark intensity maxima from the substrate. All pole figures were taken at room temperature. With the orientation, the morphology also changes (AFM micrographs, second row). (110)-oriented films ((a) and (d)) have a lower roughness then (111)-oriented or mixed films ((b) and (c)). Additionally, the feature size increases with increasing deposition temperature.

has the largest feature size, the roughness decreases again strongly (RMS = 1.36 nm). The roughness of the buffer correlates with the orientation: (111)-oriented buffers are rougher than (110)-oriented buffers. The reason for the difference in roughness lies in different surface energies: since {110} planes in bcc materials are densest packed planes, they have lower surface energies than other planes [37]. Therefore, it is energetically favorable for bcc materials to terminate with these planes, which is why the surface of (110)-oriented buffers is smooth. {111}-planes, on the other hand, have higher energies and tends to form surface facets, which increases the roughness. By adjusting the deposition temperature of the Cr buffer layer, we can tune its orientation on $Al_2O_3(0001)$ substrates. To obtain a (111)-oriented growth, only a small temperature window around 500 °C is suitable, higher and lower deposition temperatures give (110)-oriented, textured buffers. The reason for this narrow temperature range is probably the unfavorable surface energy of a {111} orientation which requires appropriate growth kinetics. To grow (111)-oriented NiTi films as a next step, we therefore chose a Cr buffer layer deposited at 500 °C.

Figure 5 summarizes the properties of a NiTi film grown on top of a Cr buffer layer on $Al_2O_3(0001)$. $Ni_{48}Ti_{52}$ was deposited at 525 °C with a thickness of 1000 nm. This deposition temperature turned out to be a trade-off, because films deposited at lower temperatures have a more pronounced R-phase transformation, while films deposited at higher temperatures start to dewet and form facets and holes due to the high surface energy of the (111)-plane. From the pole figure in figure 5(a) we can confirm that the film grows in (111)-orientation on the (111)-oriented buffer. Even though the film is mostly martensitic at room temperature, we show a B2(110) pole figure of austenite as the epitaxial relation is more difficult to see in pole figures of B19′ lattice planes. A complementary XRD measurement can be found in the supplementary (figure S3). The epitaxial relation is $Al_2O_3(0001)\,[1\bar{1}00] \parallel Cr(111)\,[2\bar{1}\bar{1}] \parallel$ NiTi B2(111) $[2\bar{1}\bar{1}]$. The transformation (figure 5(b)) goes from B2 via R-phase to B19′ during cooling and directly from B19’ to B2 during heating. The transformation temperatures are all above room temperature.

To check for possible precipitates, we performed TEM measurements on a cross section of the film (figures 5(c) and (d)). The different martensitic variants, separated by twin boundaries are visible as brighter and darker stripes (some marked with black arrows). Additionally, green arrows mark 5…10 nm wide and 50…100 nm long plates that run along B2[1 0 0] and B2[0 1 0] directions. From their orientation and appearance, they can be identified as GP-zones [34, 38]. This is in accordance with polycrystalline films, where GP zones have been observed for NiTi films with a similar composition and an annealing temperature of 500 °C [14]. No other precipitates where observed in the film. We expect that these GP zones are similar when the films are grown on MgO(100) with the same deposition conditions. We can conclude that it is possible to grow epitaxial and martensitic (111)-oriented NiTi films on $Al_2O_3(0001)$ using an optimized Cr buffer layer.

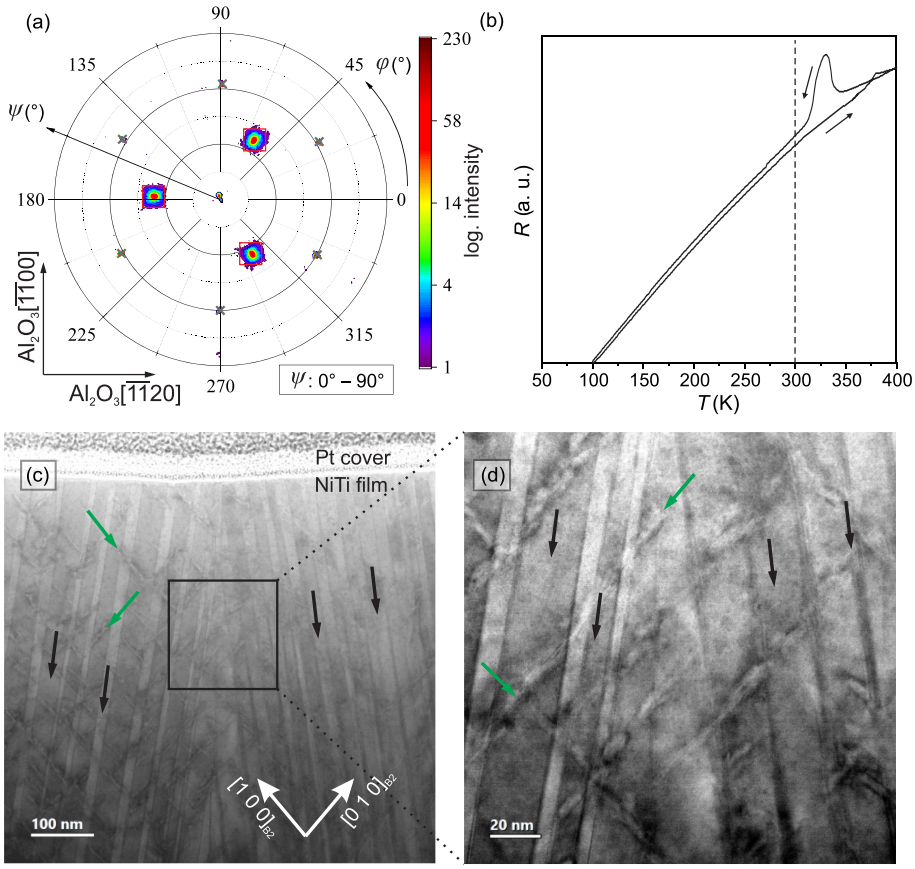

Figure 5. Orientation, transformation behavior and precipitates of a (111)-oriented $Ni_{48}Ti_{52}$ film on Al_2O_3(0001). The 1000 nm thick film was grown at 525 °C on a Cr buffer layer deposited at 500 °C. (a) The B2(110) pole figure taken at room temperature shows that the film grows epitaxially and (111)-oriented (red squares). Gray crosses mark intensities from the substrate. (b) The resistivity measurement shows the transformation behavior with a two-step transformation during cooling and a one-step transformation during heating. In both cases, the transformation temperatures are above room temperature (dotted line). (c) and (d) TEM images show the martensitic twins as bright and dark stripes (black arrows) as well as GP zone precipitates (green arrows) which are 5–10 nm thick plates that run in B2[1 0 0] and B2[0 1 0] directions.

Table 1. Growth conditions to obtain epitaxial NiTi films in (100) and (111)-orientation.

Substrate	Buffer layer	T_{Dep} NiTi	Annealing	NiTi orientation	Epitaxy relation
MgO(100)	5 nm Cr, 50 nm V; 300 °C	250 °C	2 h 650 °C , 20 min 300 °C	(100)	MgO(100) [001] ‖V(100) [011] ‖ NiTi B2 (100) [011]
MgO(100)	50 nm Cr; 500 °C	525 °C	—	(100)	MgO(100) [001] ‖ Cr(100) [011] NiTi B2 (100) [011]
Al_2O_3(0001)	50 nm Cr; 500 °C	525 °C	—	(111)	Al_2O_3(0001) [1$\bar{1}$00] ‖ Cr(111) [2$\bar{1}\bar{1}$] ‖ NiTi B2 (111) [2$\bar{1}\bar{1}$]

5. Conclusion

Epitaxially grown films, which are in a single crystalline state in austenite can be fabricated in two different orientations when suitable buffer layer and deposition conditions are used. The optimal deposition conditions are summarized in table 1. For (100)-oriented films, a 5 nm Cr and 50 nm V on MgO(100) buffer increases crystal quality and promotes better epitaxial growth of the NiTi film leading to higher transformation temperatures. For (111)-oriented films, a Cr buffer layer on Al_2O_3(0001) is needed and the buffer has to be deposited at 500 °C for (111)-oriented growth. Using optimized deposition conditions, thick epitaxial and single crystalline films in (100)- and (111)-orientation that are martensitic at room temperature are obtained. Our systematic optimization of crystallinity reveals that even small angle grain boundaries hinder martensitic transformations as they reduce the transformation temperatures. An appropriate buffer is decisive for a good crystal growth without grain boundaries, it should have a low misfit and might require optimization itself for the appropriate orientation. In future, these epitaxial NiTi films

enable experiments on the in-depth analysis of the martensitic microstructure. Moreover, they promise superior functional properties compared to polycrystalline films because instead of an ensemble average, the full spontaneous strain can be used for pseudoelastic and -plastic applications.

Data availability statement

The data that support the findings of this study are openly available at the following URL/DOI: https://doi.org/10.14278/rodare.2305 [39].

Acknowledgment

The authors acknowledge Martin F-X Wagner and Sandra Hahn for helpful discussion, Katharina Freiberg for the preparation of the TEM lamella, Carmen Weigelt for preliminary work on epitaxial NiTi films and the German Research Foundation DFG for funding through Projects FA 453/13-1, 390918228 and 134573208.

ORCID iDs

Klara Lünser https://orcid.org/0000-0003-3309-7948
Andreas Undisz https://orcid.org/0000-0001-8527-7743
Kornelius Nielsch https://orcid.org/0000-0003-2271-7726
Sebastian Fähler https://orcid.org/0000-0001-9450-4952

References

[1] Kohl M 2013 *Shape Memory Microactuators* (*Microtechnology and Mems*) (Berlin: Springer)
[2] Fu Y, Du H, Huang W, Zhang S and Hu M 2004 *Sens. Actuators* A **112** 395–408
[3] Nespoli A, Besseghini S, Pittaccio S, Villa E and Viscuso S 2010 *Sens. Actuators* A **158** 149–60
[4] Choudhary N and Kaur D 2016 *Sens. Actuators* A **242** 162–81
[5] Bechtold C, Chluba C, Lima de Miranda R and Quandt E 2012 *Appl. Phys. Lett.* **101** 091903
[6] Miyazaki S, Fu Y and Huang W (eds) 2009 *Thin Film Shape Memory Alloys—Fundamentals and Device Applications* (Cambridge: Cambridge University Press)
[7] Grummon D S and Pence T J 1996 *MRS Online Proc. Libr.* **459** 331–43
[8] Lehnert T, Crevoiserat S and Gotthardt R 2002 *J. Mater. Sci.* **37** 1523–33
[9] Gyobu A, Kawamura Y, Horikawa H and Saburi T 1996 *Mater. Trans. JIM* **37** 697–702
[10] Surbled P, Clerc C, Le Pioufle B, Ataka M and Fujita H 2001 *Thin Solid Films* **401** 52–59
[11] Gong F F, Shen H M and Wang Y N 1996 *Appl. Phys. Lett.* **69** 2656–8
[12] Otsuka K and Ren X 2005 *Prog. Mater. Sci.* **50** 511–678
[13] Kajiwara S, Ogawa K, Kikuchi T, Matsunaga T and Miyazaki S 1996 *Phil. Mag. Lett.* **74** 395–404
[14] Ishida A, Sato M, Kimura T and Sawaguchi T 2001 *Mater. Trans.* **42** 1060–7
[15] Pfetzing-Micklich J, Ghisleni R, Simon T, Somsen C, Michler J and Eggeler G 2012 *Mater. Sci. Eng.* A **538** 265–71
[16] Paul P P, Fortman M, Paranjape H M, Anderson P M, Stebner A P and Brinson L C 2018 *Shape Mem. Superelasticity* **4** 285–93
[17] Laplanche G, Pfetzing-Micklich J and Eggeler G 2014 *Acta Mater.* **68** 19–31
[18] Xiao F, Liang X, Chen H, Li Z, Li Z, Jin X and Fukuda T 2019 *Scr. Mater.* **168** 86–90
[19] Klaer P, Eichhorn T, Jakob G and Elmers H J 2011 *Phys. Rev.* B **83** 214419
[20] Niemann R, Backen A, Kauffmann-Weiss S, Behler C, Rößler U, Seiner H, Heczko O, Nielsch K, Schultz L and Fähler S 2017 *Acta Mater.* **132** 327
[21] Schwabe S, Niemann R, Backen A, Wolf D, Damm C, Walter T, Seiner H, Heczko O, Nielsch K and Fähler S 2021 *Adv. Funct. Mater.* **31** 2005715
[22] Buschbeck J, Kawasaki J, Buehl T E, Gossard A C and Palmstøm C J 2011 *J. Vac. Sci. Technol.* B **29** 03C116
[23] Buschbeck J, Kawasaki J K, Kozhanov A, James R D and Palmstrøm C J 2011 *Appl. Phys. Lett.* **98** 191901
[24] Kauffmann-Weiss S, Hahn S, Weigelt C, Schultz L, Wagner M F X and Fähler S 2017 *Acta Mater.* **132** 255–63
[25] Martins R, Schell N, Beckers M, Silva R, Mahesh K and Fernandes F B 2008 *Mater. Sci. Eng.* A **481-482** 626–9
[26] Michal G M and Sinclair R 1981 *Acta Crystallogr.* B **37** 1803–7
[27] Horcas I, Fernández R, Gómez-Rodríguez J M, Colchero J, Gómez-Herrero J and Baro A M 2007 *Rev. Sci. Instrum.* **78** 013705
[28] Jain S C, Harker A H and Cowley R A 1997 *Phil. Mag.* A **75** 1461–515
[29] Ling H C and Kaplow R 1980 *Metall. Mater. Trans.* A **11** 77–83
[30] Frenzel J, Pfetzing J, Neuking K and Eggeler G 2008 *Mater. Sci. Eng.* A **481-482** 635–8
[31] Ren X, Miura N, Zhang J, Otsuka K, Tanaka K, Koiwa M, Suzuki T, Chumlyakov Y I and Asai M 2001 *Mater. Sci. Eng.* A **312** 196–206
[32] Christian J W and Mahajan S 1995 *Prog. Mater. Sci.* **39** 1–157
[33] Matsumoto O, Miyazaki S, Otsuka K and Tamura H 1987 *Acta Metall.* **35** 2137–44
[34] Kikuchi T, Ogawa K, Kajiwara S, Matsunaga T, Miyazaki S and Tomota Y 1998 *Phil. Mag.* A **78** 467–89
[35] Nishida M, Nishiura T, Kawano H and Inamura T 2012 *Phil. Mag.* **92** 2215–33
[36] Molnárová O, Tyc O, Heller L, Seiner H and Šittner P 2021 *Acta Mater.* **218** 117166
[37] Wang S G, Tian E K and Lung C W 2000 *J. Phys. Chem. Solids* **61** 1295–300
[38] Zhang J X, Sato M and Ishida A 2003 *Acta Mater.* **51** 3121–30
[39] Lünser K, Undisz A, Nielsch K and Fähler S 2023. Data for "How to grow single-crystalline and epitaxial NiTi films in (100)- and (111)-orientation" [Data set]. Rodare. http://doi.org/10.14278/rodare.2305